Science of the Total Environment 688 (2019) 724–731

Contents lists available at ScienceDirect

Science of the Total Environment

journal homepage: www.elsevier.com/locate/scitotenv

Application of red-mud based ceramic media for phosphate uptake from water and evaluation of their effects on growth of *Iris latifolia* seedling

Nisha Shabnam [a,1], Yongtae Ahn [a,1], Aleksey Maksachev [a], Jin Hyung Lee [b], Chin-Pao Huang [c], Hyunook Kim [a,*]

[a] Department of Environmental Engineering, University of Seoul, Seoul, Republic of Korea
[b] Korea Institute of Ceramic Engineering and Technology, Jinju, Republic of Korea
[c] Department of Civil & Environmental Engineering, University of Delaware, Newark, DE, USA

HIGHLIGHTS

- A novel red-mud based ceramic media (RMCM) was developed for phosphate removal.
- Phosphate adsorption on RMCM was best described by Langmuir model.
- Pseudo first order model best described the adsorption kinetics.
- Phosphate adsorption to RMCM was endothermic, spontaneous and physisorption process.
- RMCM promoted *Iris latifolia* growth and the two together enhanced phosphate removal.

GRAPHICAL ABSTRACT

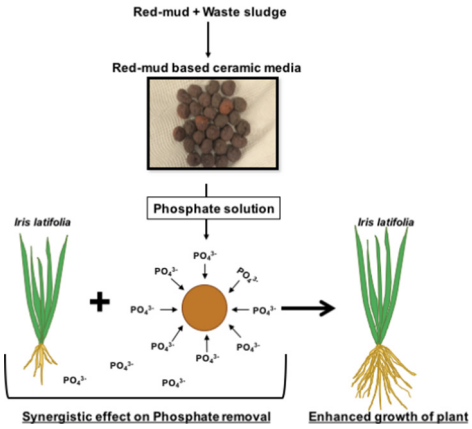

ARTICLE INFO

Article history:
Received 28 March 2019
Received in revised form 11 June 2019
Accepted 17 June 2019
Available online 19 June 2019

Keywords:
Adsorption
Ceramic
Isotherm
Kinetics
Phosphate
Red mud
Thermodynamics
Iris latifolia

ABSTRACT

In the present study, we have produced red-mud based ceramic media (RMCM) as an adsorbent for removal of phosphate from aqueous solutions, and their application in a constructed wetland. Phosphate adsorption to RMCM was investigated by varying initial phosphate concentration, contact time, and temperature. Adsorption of phosphate to the surface of RMCM was confirmed by scanning electron microscope and energy dispersive X-ray spectroscopy. The surface area and pore volume of RMCM decreased significantly after phosphate adsorption. Experimental equilibrium data followed Langmuir and Sips model better than the Freundlich model. Kinetic data followed both pseudo first order and pseudo second order reactions. Thermodynamics suggested the phosphate adsorption process onto RMCM to be endothermic and spontaneous, and physisorption dominated. Fourier transform infrared spectrumof phosphate adsorbed RMCM did not show any P—O specific bands thus ruling out role of chemical forces in phosphate adsorption. Overall, phosphate adsorption on RMCM was driven by physisorption. The RMCM promoted biomass growth and increased the surface area of roots in *Iris latifolia*. Together with RMCM, *I. latifolia* augmented removal of phosphate from aqueous solution. Based on their phosphate removal performance and plant-growth promoting effects, we believe that RMCM can be effectively used in constructed wetlands.

* Corresponding author.
E-mail address: h_kim@uos.ac.kr (H. Kim).
[1] These authors contributed equally to the paper.

https://doi.org/10.1016/j.scitotenv.2019.06.267
0048-9697/

1. Introduction

Phosphate, although being essential for living beings, can cause havoc with the environment when present at a concentration of ≥0.02 mg L^{-1} in water (Wang and Liang, 2015). It leads to eutrophication during which toxic cyanobacteria bloom to deplete oxygen levels (hypoxia), suffocate aquatic animals, and eventually disrupt the food web in aquatic bodies (Bektaş et al., 2004; Fang et al., 2017a, 2017b). Phosphate induced eutrophication has been reported to affect about 30–50% of water sources in the world (Fang et al., 2018). In humans, excess phosphate causes chronic kidney disease, cardiovascular diseases and premature ageing (Razzaque, 2011).

Agricultural run-off from fields, municipal discharge and industrial effluents are major contributors to excess phosphate in water bodies (Fang et al., 2015; Karageorgiou et al., 2007). Owing to the detrimental effects of excess phosphate on the environment and human health, it is essential to remove phosphate from the anthropogenic wastewater before their disposal into water bodies. An extensive body of research has been devoted towards development of innovative treatment technologies for effective removal of phosphate from waste effluents. These technologies include, chemical precipitation, biological methods, adsorption, crystallization, reverse osmosis and electro-coagulation (Bektaş et al., 2004; Hosni et al., 2008; Karageorgiou et al., 2007). For chemical precipitation of phosphate, salts of Al, Fe, Ca, etc. are used (Karageorgiou et al., 2007); however, this method demands a strict operation control and also carries with it the risk of release of Cl^- and SO_4^{2-} into water (Yao et al., 2011). Prospective use of nanomaterials has also been tested for removal of phosphate from water (Fang et al., 2015, 2017b). Biological treatment technologies exploit living organisms like bacteria, fungi, and plants, which use phosphate as an energy source for biomass growth (Wang et al., 2016). Both chemical and biological methods demand large capital investment and pose the problem of disposal of phosphate-rich sludge generated after the treatment (Yao et al., 2011; Wang et al., 2016). Moreover, while chemical methods are inefficient for treatment of water with trace levels of phosphate (Huang et al., 2009; Lǔ et al., 2013), effectiveness of biological methods is also unrealistic (Yildiz, 2004; Bektaş et al., 2004). Due to their high cost-demand, treatment technologies like reverse osmosis, ion exchange, and electrodialysis are not practically applicable (Mor et al., 2016). Although crystallization of phosphate as hydroxyapatite and/or struvite using salts under an alkaline condition is a promising approach as it resolves the issue of sludge disposal and PO_4^- recovery, it is also economically too expensive to be approachable for commercial purpose (Dai et al., 2016; Zhao et al., 2019). Among all the techniques developed so far, adsorption still remains the most popular and cost-effective method for removal of phosphate (Dai et al., 2011; Fang et al., 2017a, 2017b). Various adsorbents have been developed ranging from (i) natural materials like dried plant biomass, animal shells, etc.; (ii) synthetic materials like zeolites, alumina, metal/metal-oxide nanoparticles, etc.; and (iii) industrial wastes and residuals like fly ash, blast furnace slag, dewatered alum sludge, red mud, skin split waste, etc. (Dai et al., 2011; Huang et al., 2009; Lǔ et al., 2013; Wang et al., 2016).

Red mud is an alkaline byproduct formed during production of alumina from bauxite (Huang et al., 2008). It is estimated that 1–2 tons of red mud is generated for every ton of alumina produced (Huang et al., 2008). Due to its chemical stability, red mud has been extensively used to control soil leaching and adsorb nutrients (including phosphate), heavy metals, phenols, etc. in wastewater and acid mine leachates (Huang et al., 2008; Sahu et al., 2013). However, the fine powdered texture of red mud will block water flow, thus making it unsuitable for practical applications in a built environment such as constructed wetlands (López-García et al., 2017).

In this study, therefore, we have developed a novel red-mud-based ceramic medium (RMCM), keeping in mind their practical applications in phosphate removal or recovery. Unlike previous studies with red mud, we made the RMCM in a pelletized form, so they could be used as building blocks in a constructed wetland. We investigated the potential of RMCM to adsorb phosphate as a function of initial phosphate concentration, contact time and temperature, and mathematical models were used to simulate the experimental data. Phosphate adsorption on RMCM was characterized using scanning electron microscope (SEM), energy dispersive X-ray spectroscopy (EDS) and Fourier transform infrared spectroscopy (FT-IR). The potential use of RMCM in constructed wetlands was evaluated by measuring its impact on phosphate uptake by *Iris latifolia* (a wetland plant). Our results show that the new designed RMCM can effectively adsorb phosphate. The synergistic effects of RMCM and *I. latifolia* plants on phosphate removal make RMCM an ideal material for application in constructed wetlands.

2. Materials

All the chemicals used in this study are analytical grade and were provided by Duksan chemicals, Seoul, Korea. Red mud was provided by Hongju Company, Guangju, Korea.

2.1. Methods

2.1.1. Synthesis and characterization of RMCM

Mixture consisting of Ocher (30%), clay (31%), kaolin (10%), red mud (15%), zeolite (11%), and volcanic corroded soil (3%) were mixed in sludge slurry to make dough. The dough was then shaped into cylindrical forms (length: 25–33 mm; diameter: 15–17 mm) which were subsequently dried, and thereafter fired at 850–950 °C for 1 h followed by cooling. These cylindrical-shaped media were used for further experiments. More detailed information about RMCM is provided as supporting information (SI-S1).

The surface and composition of RMCM were characterized using SEM and EDS. For SEM and EDS studies, RMCM were washed with deionized water and dried at 95 °C. Surface of a part of the dried media was uniformly coated with Pt—Pd using Hitachi MC1000 ion sputter (Hitachi, Tokyo, Japan) and then viewed under Hitachi S-8220 field emission SEM-EDS (Hitachi, Tokyo, Japan).

For FT-IR studies, the surface of the RMCM was scratched to collect a fine powder. This powder was then used to obtain FT-IR data using a Nicolet iN10 Mx FT-IR microscope (Thermo Scientific, Waltham, MA, USA).

To determine the surface area and pore volume of RMCM, N_2 adsorption-desorption isotherm measurements were performed by Micromeritics sorption analyzer (Model ASAP-2400, Micrometrics, Norcross, GA, USA) at 77 K and 273 K. Prior to the measurements, RMCM samples were activated at 673 K under vacuum. The surface area and pore volume were calculated using the Brunauer-Emmett-Teller (BET) equation (Brunauer et al., 1938) and the Barrett-Joyner-Halenda (BJH) equation (Barrett et al., 1951), respectively.

2.1.2. Adsorption experiments

Phosphate adsorption by RMCM was studied in a series of batch experiments. Effects of various parameters such as initial phosphate concentration, contact time, temperature, and pH on adsorption of phosphate to RMCM were evaluated. For the present study, KH_2PO_4 was used as phosphate salt.

For a typical batch adsorption experiment, RMCM was washed thoroughly 4–5 times with deionized water. After washed, the media were dried in an oven at 90 °C for 3 d to completely remove water. Batch experiments were carried in 300-mL Erlenmeyer flasks. Each flask containing 25 g RMCM in 250 mL of phosphate solution was sealed with parafilm. The flasks were placed in an orbital shaker and continuously shaken at 120 rpm.

Kinetics experiments were carried out at an initial concentration of 100 mg L^{-1} under a constant temperature of 25 °C and pH equivalent to 7; thermodynamics studies were performed at 15 °C, 25 °C and 45 °C using different concentrations of phosphate at pH 7. For studying

the effect of pH, NaOH or HCl was used to adjust solution pH to 3, 5, 7, or 9. At a fixed interval, aliquots were taken from flasks, filtered using a 0.45-μm cellulose acetate filter (Advantec, Toyo Roshi Kaisha, Tokyo, Japan), and analyzed for phosphate content using ion chromatography (883 Basic IC plus; column: Metrosep A Supp4-250/4.0; Methrom, Herisau, Switzerland). The eluent consisting of 3.2-mM sodium carbonate (Na_2CO_3) and 1.0-mM sodium bicarbonate ($NaHCO_3$) was delivered at a flow rate of 0.7 mL min^{-1}.

The amount of phosphate adsorbed onto RMCM at equilibrium, q_e (mg kg^{-1}), was obtained using the following equation:

$$q_e = \left[\frac{C_o - Ce}{M}\right] V \quad (1)$$

where C_o and C_e are the initial and equilibrium PO_4^{3-} concentrations (mg L^{-1} of PO_4^{3-}), respectively; M refers to the mass of RMCM (25 g) used and V does to the volume of PO_4^{3-} solution (mL).

Desorption experiments were conducted using phosphate saturated RMCM (adsorbed phosphate was ~ 420 mg kg^{-1}). Phosphate saturated RMCM was incubated in 250 mL of double distilled water (pH of 7) in Erlenmyer flask and placed on an orbital shaker with a constant speed of 120 rpm at a constant temperature of 25 °C for 24 h.

2.1.3. Effect of RMCM on phosphate adsorption by I. latifolia

Seedlings of *I. latifolia* were raised in garden soil under a photon flux density of 120 μmol photons m^{-2} s^{-1} (10/14 h light/dark cycle) at 25 ± 2 °C in a plant growth chamber (MLR-352-H-PA, Panasonic, Gunma, Japan). For the phosphate treatment, seedlings were washed carefully to remove soil particles. Seedlings were, then, transferred to tubes containing 50 mL phosphate solution (150 or 450 mg L^{-1}) in the absence and presence of RMCM (5 g) with their roots immersed in the solution. Distilled water was used as a control. The tubes containing plants along with media and the respective controls were incubated at 25 ± 2 °C under a photon flux density of 120 μmol photons m^{-2} s^{-1} (10/14 h light/dark cycle) for 3 weeks. In the case of tubes with plants, phosphate solutions were replenished with distilled water every day. Phosphate levels were determined in the residual solutions as described above. To determine the dry biomass, plants were washed with distilled water. Roots and shoots were separated and dried in an oven at 90 °C for 2 d. The samples were weighed after cooling.

2.1.4. Statistics

All the data are presented as mean ± standard error ($\rho = 0.05$). All experiments were repeated minimum 4 times each with 3 replicates.

3. Results and discussion

3.1. Surface characteristics of RMCM

Surface morphology and elemental characteristics of RMCM before and after phosphate adsorption were analyzed using SEM and the results are depicted in Fig. 1. Surface of the RMCM was rough (Fig. 1A), composed of many aggregated particles. No major visible difference was noticeable in the surface morphology of RMCM after phosphate adsorption (Fig. 1B). EDS analysis of both pristine and phosphate treated RMCM showed peaks specific to elements Fe, Al, Si, Na, Ca which are the main components of red mud as described in the literature (Huang et al., 2008; Sahu et al., 2013). However, the EDS spectra of the pristine composite does not show any phosphorous-specific peak, which was very prominent in the case of phosphate-treated media (Fig. 1C,D). This confirms successful adsorption of phosphate onto the media. It is also evident from the elemental mapping of phosphorus (through EDS) that phosphate was adsorbed onto the surface of RMCM (Fig. 1E,F).

Qualitative analysis of phosphate adsorption by RMCM was also carried out through FT-IR studies. Fig. 2 depicts the FT-IR spectra of RMCM before and after phosphate adsorption. Phosphate-treated RMCM did not show any alteration in the spectra compared to the pristine RMCM; no distinct bands corresponding to the P—O stretch vibrations were noted. These results further suggested that chemical forces were not involved in the adsorption of phosphate on RMCM.

The N_2 adsorption-desorption isotherms for RMCM samples are shown in Fig. 3.

RMCM displayed a type-IV isotherm with an H3 hysteresis loop at relative pressures of 0.59–1.0. As per International Union of Pure and Applied Chemistry, it is inferred from the isotherm that RMCM has mesoporous characteristics with slit shaped pores (Lei et al., 2017; Zheng et al., 2017). The surface area of pristine RMCM was 1.049 m^2 g^{-1}, which reduced to 0.693 after phosphate adsorption. Similarly, pore volume of the phosphate saturated RMCM declined to 0.0014 cm^3 g^{-1} from the initial value of 0.0061 cm^3 g^{-1}. The decrease in surface area of RMCM post phosphate adsorption can be attributed to aggregation and overlapping of the adsorption sites on surface of RMCM (Mahmoodi et al., 2011).

3.2. Adsorption isotherm

The adsorption capacity of pristine RMCM increased with the increase of phosphate concentration until an equilibrium was attained at 200 mg L^{-1}. The adsorption capacity at equilibrium was ~ 420 mg kg^{-1}. The removal capacity for phosphate decreased from over 90% at concentrations of ≤5 mg L^{-1} to ~16% at 200 mg L^{-1}. The lower P removal efficiency of RMCM at high concentrations can be attributed to a decrease in the available surface area. Decrease in the removal efficiency at high concentrations was also attributed to the fact that for a given dose, the number of sites for adsorption are fixed, thus, resulting in adsorption of the same amount of adsorbate (Mezenner and Bensmaili, 2009). Desorption studies revealed that phosphate saturated RMCM (~ 420 mg kg^{-1}) could desorb ~9% of the adsorbed phosphate which was equivalent to ~ 36.9 mg kg^{-1}.

The experimental equilibrium data of phosphate adsorption by RMCM were fitted to the Langmuir, Freundlich, and hybrid Langmuir-Freudlich (Sips) isotherm models (Fig. 4). The Langmuir isotherm assumes monolayer adsorption to homogenous surface with a fixed number of adsorption sites (Langmuir, 1916). After a site is filled, no further adsorption occurs on it. The Langmuir isotherm is expressed by the following equation:

$$q_e = \frac{q_m b C_e}{1 + bC_e} \quad (2)$$

where q_m (mg kg^{-1}) is the maximum amount of phosphate adsorbed by an adsorbent, resulting in complete monolayer coverage and b (L mg^{-1}) is the Langmuir constant that corresponds to free energy of adsorption. q_e refers to the amount of phosphate adsorbed onto RMCM at equilibrium and C_e is the equilibrium phosphate concentration (Eq. (1)).

The Freundlich isotherm assumes multilayer adsorption to heterogenous surface (Freundlich, 1906) and is represented by the following equation:

$$q_e = K_f . C_e^{1/n} \quad (3)$$

where K_f (mg $L^{-1/n}$ g^{-1} $L^{1/n}$) is the Freundlich constant, $1/n$ is the heterogeneity factor which denotes the adsorption capacity and intensity of an adsorbent. The surface site heterogeneity increases as n approaches zero. The n values for phosphate adsorption on RCMC were >1, indicating that adsorption is favorable.

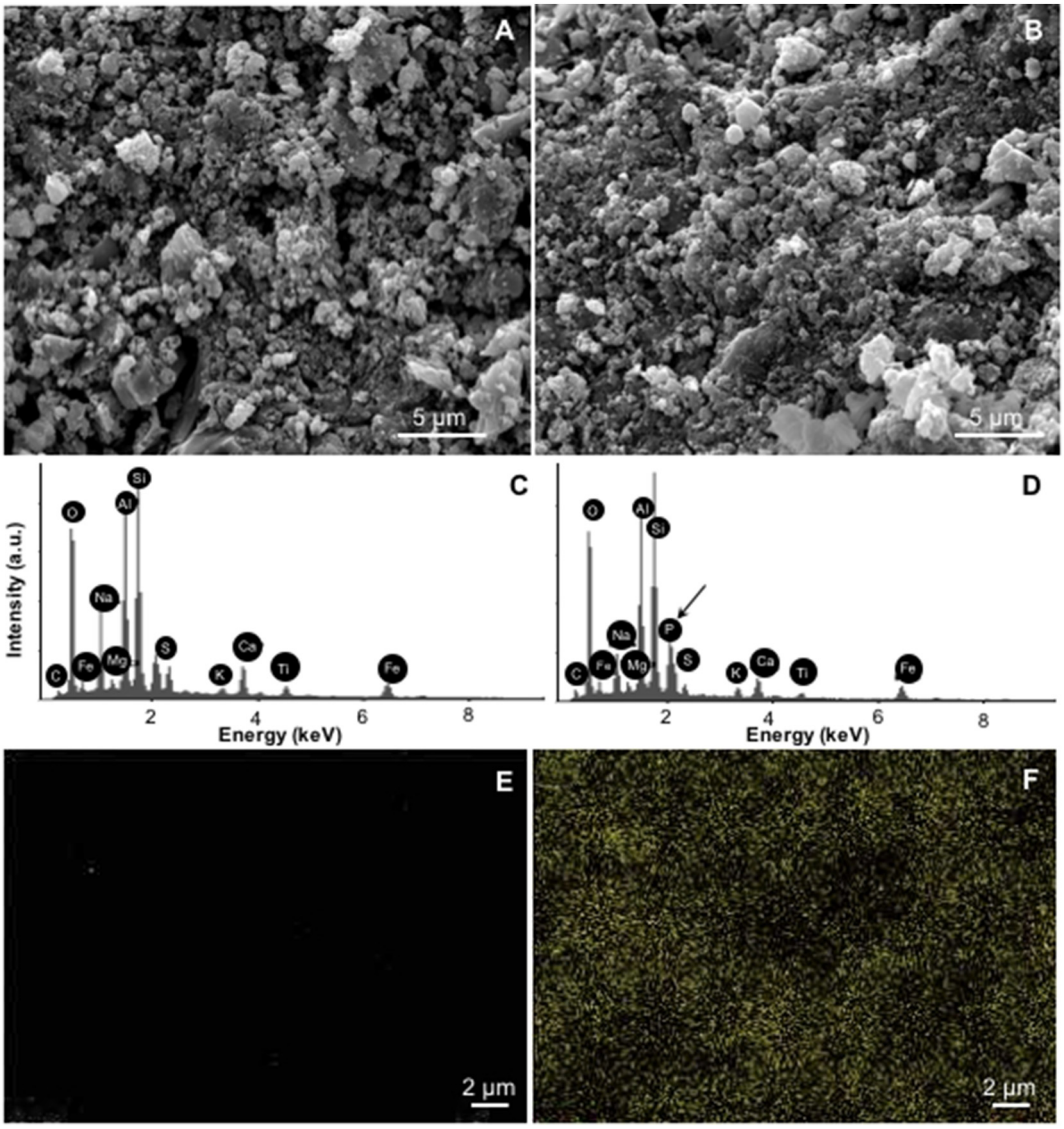

Fig. 1. SEM images (A,B), and EDS (C,D) and phosphorous elemental map (E,F) of pristine (A,C,E) and phosphate adsorbed (B,D,F) RMCM. Yellow dots represent phosphorous. (For interpretation of the references to color in this figure legend, the reader is referred to the web version of this article.)

The equation for the Sips model (Sips, 1948) is given as:

$$q_e = q_m \frac{C_e^m}{K_s + C_e^m} \quad (4)$$

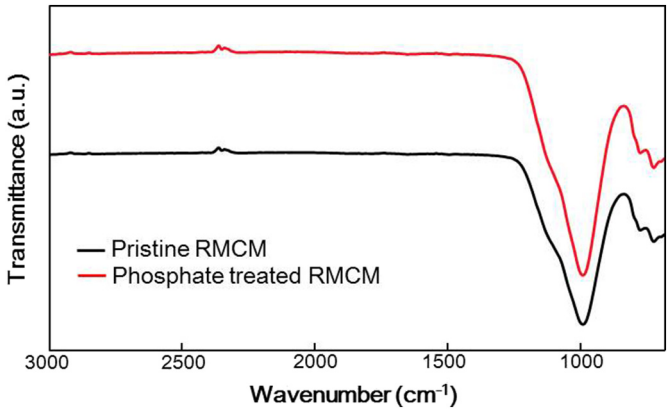

Fig. 2. FT-IR spectrum of RMCM before and after adsorption of phosphate.

where q_m (mg g^{-1}) is the maximum adsorption capacity, K_S $(L\ mg^{-1})^{1/m}$ is the Sips constant corresponding to energy of adsorption and m denotes the heterogeneity of an adsorption system; m is directly proportional to the system heterogeneity (Sips, 1948). The heterogeneity factor (m) differentiates Sips from Langmuir equation; when $n = 1$, the Sips equation is reduced to the Langmuir equation denoting that the surface is homogenous.

Fitted parameters of the Langmuir, Freundlich and Sips models for phosphate adsorption by RMCM and the coefficient of determination (R^2) value for each isotherm are given in Table 1. As evident from R^2 values in Table 1, experimental data relatively well fit all to the Langmuir and Sips models than Freundlich model. As mentioned above, Langmuir isotherm assumes the presence of monolayer adsorption sites, while Freundlich isotherm assumes surface heterogeneity. However, it is very important to focus that these isotherm models are based on gaseous equilibrium between the adsorbent and the adsorbate. These models were extended to liquid-solid equilibrium assuming that there is very dilute concentration of adsorbate. It is well accepted that at low concentrations of adsorbate, Sips isotherm is reduced to Freundlich isotherm and at high concentrations, it follows a monolayer adsorption capacity similar to Langmuir isotherm (Hokkanen et al., 2015). In the present study, the m value is 1.45, which rules out the

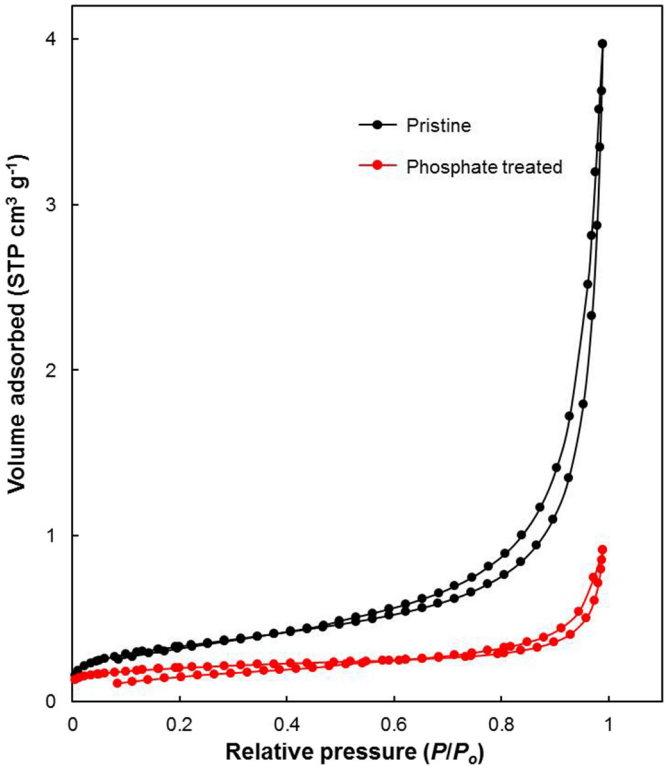

Fig. 3. Nitrogen adsorption-desorption isotherms at 77 K on RMCM before (a) and after (b) phosphate adsorption.

heterogenous adsorption character (Nethaji et al., 2013). Probably, the high temperature applied (> 1000 °C; see the supplementary information) during the synthesis of RMCM, decomposes organic compounds and hydroxyl groups in the material and reduces the surface roughness, as reported by others (e.g., Doğan et al., 2000; Wang et al., 2005). Thus, it can be concluded that phosphate adsorption on RMCM is a monolayer adsorption process on homogenous surface which is best described by Langmuir model.

3.3. Adsorption kinetics

Kinetics of phosphate adsorption to RMCM were evaluated by performing a series of batch experiments in which 100 mg L^{-1} phosphate was used for 25 g RMCM. The phosphate adsorption by RMCM as a function of time is shown in Fig. 5. Adsorption of phosphate by RMCM increased with time until an equilibrium was attained. As seen in Fig. 5, the amount of phosphate adsorbed by RMCM increased within the first 8 h, beyond which no further significant change was noted in adsorption capacity. Hence, for the initial concentration of 100 mg L^{-1}, the optimal equilibrium adsorption time was 8 h. This suggests that increase in adsorption during the initial stage of 0–8 h could be due to presence of abundant active sites available on the surface of RMCM. The non-significant change in phosphate adsorption after 8 h suggests that all the active adsorption sites on RMCM have become saturated (Wang et al., 2015).

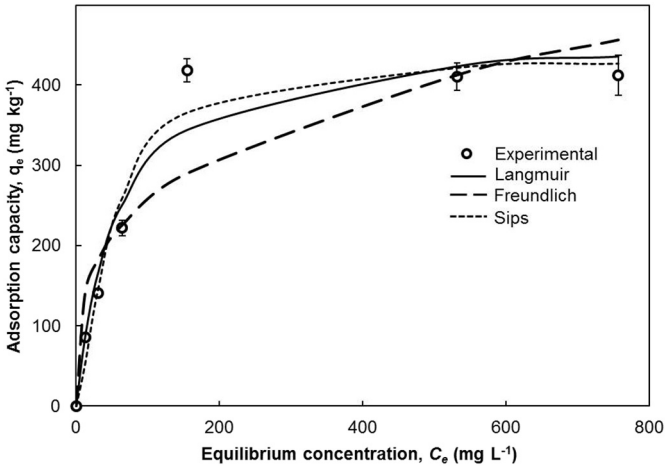

Fig. 4. Adsorption isotherms phosphate to RMCM. Contact time: 24 h; adsorbate volume: 250 mL; adsorbent dose: 25 g; temperature: 25 ± 1 °C; shaking speed: 15 rpm. Data are represented as mean ± standard error (a vertical line on each datum point).

Table 1
Isotherm constants for phosphate adsorption to RMCM. Contact time: 24 h; volume of water sample: 250 mL; adsorbent dose: 25 g; temperature: 25 ± 1 °C; shaking speed: 15 rpm.

Isotherm	Isotherm constants	
Langmuir	q_m (mg kg^{-1})	467
	b (L mg^{-1})	0.018
	R^2	0.96
Freundlich	K_F (mg kg^{-1})(L $mg^{-1})^{1/n}$	69
	$1/n$	0.29
	R^2	0.87
Sips	q_m (mg kg^{-1})	435
	K_s	0.004
	m	1.45
	R^2	0.97

The experimental kinetics data were fitted to the Lagergren pseudo-first-order model and pseudo-second-order kinetic models to assess the adsorption mechanism(s). The pseudo first order kinetic equation is expressed as:

$$log(q_e - q_t) = logq_e - \frac{K_1 t}{2.303} \quad (5)$$

where q_t and q_e (mg kg^{-1}) refer to the amount of PO_4^{3-} adsorbed at a given time (t min) and at equilibrium, respectively; K_1 (min^{-1}) represents the adsorption rate constant. The slope and intercept of the linear plot of log (q_e-q_t) vs t gives the value for K_1 and q_e, respectively.

On the other hand, the pseudo second order model is expressed as follows:

$$\frac{t}{q_t} = \frac{1}{K_2 q_e^2} + \frac{t}{q_e} \quad (6)$$

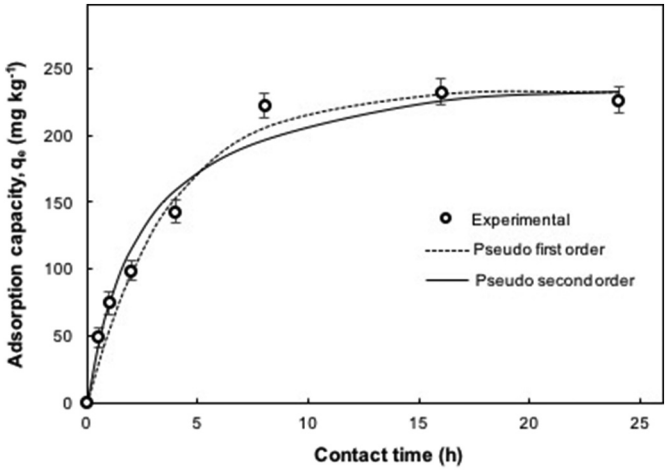

Fig. 5. Kinetics of phosphate adsorption to RMCM. Initial concentration: 100 mg L^{-1}; adsorbate volume: 250 mL; adsorbent dose: 25 g; temperature: 25 ± 1 °C; shaking speed: 15 rpm. Data are represented as mean ± standard error (a vertical line on each datum point).

where K_2 (g mg^{-1} min^{-1}) refers to the constant for the pseudo second order rate reaction. q_e is obtained from the slope of linear plot of t/q_t vs t, K_2 is deduced from the intercept. Fitting of the pseudo first order model and pseudo second order one to experimental data is depicted in Fig. 5.

Kinetic parameters for the phosphate adsorption to RMCM obtained using the two models are depicted in Table 2. While the pseudo-first-order model is widely used for reversible reactions in which a equilibrium is established between liquid and solid phases, the pseudo-second-order model defines a chemisorption processes involving valency forces through the sharing or exchange of electrons between the adsorbent and adsorbate (Radnia et al., 2011). Apparently, both kinetic models could well describe the experimental data, with R^2 exceeding 0.99. A similar finding was reported by Jung et al. (2015) wherein experimental data for phosphate adsorption on biochar/Mg-Al assembled nanocomposites was good fit to both the models. Yao et al., (2011) also noted that phosphate adsorption by biochar (derived from sugar beet tailings) followed both pseudo first order and pseudo second order kinetic models, with R^2 values exceeding 0.99. Nonetheless, residuals from the data fit with the pseudo-first-order model are less biased (Fig. 5). Therefore, it can be stated that the pseudo-first-order model better fits the data than the pseudo-second-order one.

3.4. Thermodynamics studies of phosphate adsorption onto RMCM

Effect of temperature on the adsorption of phosphate by RMCM was studied at three temperatures: 15, 25, and 45 °C. Only small difference was noted between the adsorption capacity of RMCM for phosphate at 15 °C (185 mg kg^{-1}) and at 25 °C (Fig. 6); the maximum phosphate adsorption capacity of RMCM was 185 and 222 mg kg^{-1} at 15 and 25 °C, respectively. However, the phosphate adsorption capacity of RMCM was significantly enhanced at 45 °C; it was estimated ~ 670 mg kg^{-1}. Moreover, at 45 °C, the adsorption system reached at equilibrium with an initial concentration of 100 mg L^{-1}, while at 15 or 25 °C, it did at 200 mg L^{-1}. These results proved that high temperature would be favorable for adsorption of phosphate to RMCM. The enhanced phosphate adsorption at a higher temperature can be attributed to higher diffusion and mobility rates of ions at high temperatures (Hodaifa et al., 2013).

Thermodynamic properties for the phosphate adsorption to RMCM, namely free energy change (ΔG°), enthalpy change ($\Delta H°$), and entropy change ($\Delta S°$) were calculated with the following equations:

$$\Delta G^\circ = -RT\log K_c \quad (7)$$

where R is the universal gas constant (8.314 J mol^{-1} K^{-1}), K is absolute temperature (K), K_c is the equilibrium constant. K_c is determined from:

$$K_C = \frac{1000 q_e}{C_e} \quad (8)$$

ΔH° and $\Delta S°$ were determined from following equation:

$$\log K_C = -\frac{\Delta H^\circ}{RT} + \frac{\Delta S^\circ}{R} \quad (9)$$

ΔH° is deduced from slope and $\Delta S°$ from intercept of the linear plot of log K_C vs $1/T$, respectively. The thermodynamic parameters for phosphate adsorption onto RMCM are presented in Table 3. The negative $\Delta G°$ value indicates that the adsorption of phosphate to RMCM is thermodynamically favorable and spontaneous. Increase of $\Delta G°$ with temperature reveals that spontaneity of the adsorption process is enhanced at higher temperatures. Magnitude of $\Delta G°$ determines if the adsorption is a chemisorption or physisorption process; physisorption is defined when $\Delta G°$ is determined between 0 and −20 kJ mol^{-1} and chemisorption is determined when $\Delta G°$ is between −80 to −400 kJ mol^{-1} (Wimalasiri et al., 2015). In the present study, the $\Delta G°$ values (Table 3) are more negative than −20 kJ mol^{-1} but close to the range of $\Delta G°$ values for a physisorption process, suggesting that the adsorption of phosphate on RMCM obeys physisorption more than chemisorption. Similar findings have been reported in studies of phosphorous removal by La(OH)$_3$-modified exfoliated vermiculites (Huang et al., 2014) and adsorption of carbofuran on biochars from tea waste and rice husk (Vithanage et al., 2016). The positive $\Delta H°$ (i.e., 24.38 kJ mol^{-1}) suggests that the reaction is endothermic which is also corroborated by the increased adsorption capacity of RMCM at a higher temperature. The positive $\Delta S°$ (i.e., 0.17 J mol^{-1} K^{-1}) suggests increased randomness at the interface of RMCM-phosphate solution system during the adsorption process. This can be due to the fact that the number of desorbed water molecules are higher than that of the adsorbed phosphate ions thus resulting in an increase in entropy (Anastopoulos and Kyzas, 2016; Li et al., 2005). Based on (i) thermodynamics analysis which revealed phosphate adsorption on RMCM to be a physisorption dominated process; and (ii) absence of role of chemical forces in phosphate adsorption as evidenced by FT-IR studies, we suggest that pseudo first order is more applicable for the kinetic studies.

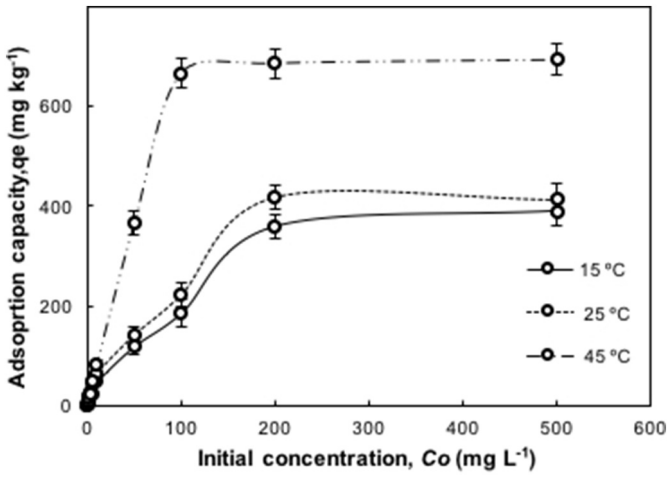

Fig. 6. Isotherms of phosphate adsorption to RMCM at different temperatures. Contact time: 24 h; adsorbate volume: 250 mL; adsorbent dose: 25 g; pH: 7; shaking speed: 15 rpm. Data are represented as mean ± standard error (a vertical line on each datum point).

3.5. Synergistic effect of RMCM and I. latifolia on removal of phosphate

Since the RMCM had been designed for its implementation in constructed wetlands and plants are an indispensable component of wetlands, investigations were carried to evaluate the role of a wetland plant, *I. latifolia* in phosphate removal by RMCM. Interestingly, RMCM treatment, irrespective of the phosphate treatment, resulted in

Table 2
Kinetic model parameters for phosphate adsorption to RMCM. Contact time: 24 h; volume of water sample: 250 mL; adsorbent dose: 25 g; temperature: 25 ± 1 °C; shaking speed: 15 rpm.

	q_e	$K_f' 10^{-2}$	R^2
First order	230 mg kg^{-1}	0.45 min^{-1}	0.994
Second order		0.27 g mg^{-1} min^{-1}	0.993

Table 3
Thermodynamic parameters for phosphate adsorption to RMCM. Contact time: 24 h; volume of water sample: 250 mL; adsorbent dose: 25 g; pH: 7; shaking speed: 15 rpm.

Temperature (°C)	ΔG (kJ mol^{-1})	ΔH (kJ mol^{-1})	ΔS (J mol^{-1} K^{-1})
15 °C	−24.2	24.4	0.17
25 °C	−27.6		
45 °C	−29.6		

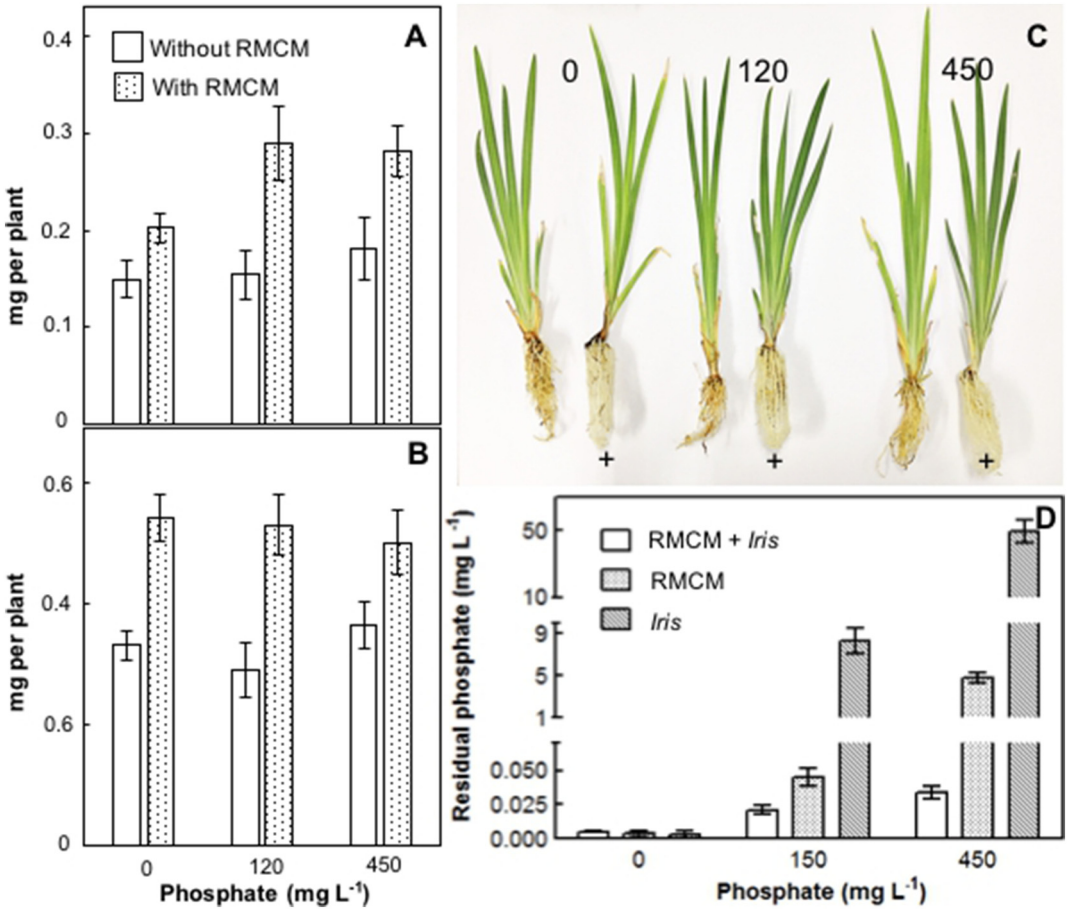

Fig. 7. Effect of RMCM on phosphate uptake by *Iris latifolia*. Dry weight (A,B) of root (A) and shoot (B); and phenotype (C) of plants of *I. latifolia* in absence and presence (+) of RMCM. Residual phosphate in solutions incubated with phosphate solutions in absence and presence of RMCM (D).

enhanced biomass in the plants (Fig. 7 A,B). These results revealed that RMCM has a promoting effect on the growth of *I. latofilia*. Moreover, surface area of roots of *I. latifolia* grown in the presence of RMCM was larger (due to fibrous roots) compared to those raised in the absence of RMCM. A large root system and high number of fibrous roots help in oxidizing the rhizosphere to a greater extent and increase their availability to pollutants (Hyland et al., 2015; Weis and Weis, 2004).

The potential of *I. latifolia* in removing phosphate was significantly lower than RMCM (Fig. 7D). However, on the mass basis, the phosphate removal efficiency of *I. latifolia* was ~25 times higher than that of RMCM. Overall, the total amount of phosphate removed by *I. latifolia* and RMCM together was significantly higher than that by RMCM and plants individually (Fig. 7). Owing to the positive effects of RMCM on the plant, we believe that RMCM would be an effective material for removal of phosphate in constructed wetlands where plants like *I. latifolia* are grown.

4. Conclusions

In this study, we have designed RMCM as a novel adsorbent for phosphate. Adsorption studies revealed that the maximum adsorption capacity of RMCM for phosphate was ~ 420 mg kg^{-1}. Scanning electron microscopy, energy dispersive spectroscopy and FT-IR analyses confirmed the adsorption of phosphate on the surface of RMCM. Phosphate adsorption onto RMCM was analyzed using adsorption isotherms, kinetic models, and thermodynamics. Equilibrium adsorption parameters derived from the adsorption isotherms suggested that phosphate adsorption on RMCM is a monolayer adsorption process on homogenous surface, best described by the Langmuir model. Thermodynamic parameters like $\Delta G°$, $\Delta H°$, and $\Delta S°$ suggested the adsorption process to be an endothermic and spontaneous. FT-IR analysis ruled out the involvement of chemical forces in phosphate adsorption process. Although the adsorption kinetics followed both pseudo first and second order models, it could be described as a physisorption dominated process. Hence, pseudo first order model best described the adsorption kinetics. RMCM promoted the growth of *I. Latifolia* and yielded a larger root system with a higher number of fibrous roots. *I. Latifolia*, together with RMCM enhanced the removal of phosphate. Based on their phosphate adsorption capacity and positive effect on *I. latifolia*, we believe, RMCM can be effectively used for removal of phosphate in constructed wetlands.

Acknowledgements

This work was supported by Korea Ministry of Environment (MOE; Project No-2015001790002), which is greatly appreciated.

Appendix A. Supplementary information

Supplementary data to this article can be found online at https://doi.org/10.1016/j.scitotenv.2019.06.267.

References

Anastopoulos, I., Kyzas, G.Z., 2016. Are the thermodynamic parameters correctly estimated in liquid-phase adsorption phenomena? J. Mol. Liq. 218, 174–185.
Barrett, E.P., Joyner, L.G., Halenda, P.P., 1951. The determination of pore volume and area distributions in porous substances. I. Computations from nitrogen isotherms. J. Am. Chem. Soc. 73, 373–380.
Bektaş, N., Akbulut, H., Inan, H., Dimoglo, A., 2004. Removal of phosphate from aqueous solutions by electro-coagulation. J. Hazard. Mater. 106, 101–105.

Brunauer, S., Emmett, P.H., Teller, E., 1938. Adsorption of gases in multimolecular layers. J. Am. Chem. Soc. 60, 309–319.
Dai, J., Yang, H., Yan, H., Shangguan, Y., Zheng, Q., Cheng, R., 2011. Phosphate adsorption from aqueous solutions by disused adsorbents: chitosan hydrogel beads after the removal of copper(II). Chem. Eng. J. 166, 970–977.
Dai, H., Lu, X., Peng, Y., Zou, H., Shi, J., 2016. An efficient approach for phosphorus recovery from wastewater using series-coupled air-agitated crystallization reactors. Chemosphere 165, 211–220.
Doğan, M., Alkan, M., Onganer, Y., 2000. Adsorption of methylene blue from aqueous solution onto perlite. Water Air Soil Pollut. 120 (3–4), 229–248.
Fang, L., Huang, L., Holm, P.E., Yang, X., Hansen, H.C.B., Wang, D., 2015. Facile upscaled synthesis of layered iron oxide nanosheets and their application in phosphate removal. J. Mater. Chem. A 3, 7505.
Fang, L., Wu, B., Lo, I.M.C., 2017a. Fabrication of silica-free superparamagnetic ZrO_2@Fe_3O_4 with enhanced phosphate recovery from sewage: performance and adsorption mechanism. Chem. Eng. J. 319, 268-267.
Fang, L., Shi, Q., Nguyen, J., Wu, B., Wang, Z., Lo, I.M.C., 2017b. Removal mechanisms of phosphate by lanthaum hydroxide nanorods: investigations using EXAFS, ATR-FTIR, DFT, and surface complexation modeling approaches. Environ. Sci. Technol. 51, 12377–12384.
Fang, L., Liu, R., Li, J., Xu, C., Huang, L.-Z., Wang, D., 2018. Magnetite/lanthanum hydroxide for phosphate sequestration and recovery from lake and the attenuation effects of sediment particles. Water Res. 130, 243–254.
Freundlich, H., 1906. Adsorption in solution. Phys. Chem. Soc. 40, 1361–1368.
Hodaifa, G., Ochando-Pulido, J.M., Alami, S.B.D., Rodriguez-Vives, S., Martinez-Ferez, A., 2013. Kinetic and thermodynamic parameters of iron adsorption onto olive stones. Ind. Crop. Prod. 49, 526–534.
Hokkanen, S., Repo, E., Lou, S., Sillanpää, M., 2015. Removal of arsenic (V) by magnetic nanoparticle activated microfibrillated cellulose. Chem. Eng. J. 260, 886–894.
Hosni, K., Moussa, S.B., Chachi, A., Amor, M.B., 2008. The removal of PO_4^{3-} by calcium hydroxide from synthetic wastewater: optimisation of the operating conditions. Desalination 223, 337–343.
Huang, W., Wang, S., Zhu, Z., Li, L., Yao, et al., 2008. Phosphate removal from wastewater using red mud. J. Hazard. Mater. 158, 35–42.
Huang, X., Liao, X., Shi, B., 2009. Adsorption removal of phosphate in industrial wastewater by using metal-loaded skin split waste. J. Hazard. Mater. 166, 1261–1265.
Huang, W.-Y., Li, D., Liu, Z.-Q., Tao, Q., Zhu, Y., Yang, J., Zhang, Y.-M., 2014. Kinetics, isotherm, thermodynamic, and adsorption mechanism studies of La(OH)3-modified exfoliated vermiculites as highly efficient phosphate adsorbents. Chem. Eng. J. 236, 191–201.
Hyland, K.C., Blaine, A.C., Higgins, C., 2015. Accumulation of contaminants of emerging concern. Environ. Toxicol. Chem. 34, 2222–2230.
Jung, K.W., Jeong, T.U., Hwang, M.J., Kim, K., Ahn, K.H., 2015. Phosphate adsorption ability of biochar/Mg–Al assembled nanocomposites prepared by aluminum-electrode based electro-assisted modification method with MgCl2 as electrolyte. Bioresour. Technol. 198, 603–610.
Karageorgiou, K., Paschalis, M., Anastassakis, G.N., 2007. Removal of phosphate species from solution by adsorption onto calcite used as natural adsorbent. J. Hazard. Mater. 139, 447–452.
Langmuir, I., 1916. The constitution and fundamental properties of solids and liquids part I solids. J. of Am. Chem. Soc. 38, 2221–2295.
Lei, C., Zhu, X., Zhu, B., Jiang, C., Le, Y., Yu, J., 2017. Superb adsorption capacity of hierarchical calcined Ni/Mg/Al layered double hydroxides for Congo red and Cr(VI) ions. J. Hazard. Mater. 321, 801–811.
Li, Y.-H., Di, Z., Ding, J., Wu, D., Luan, Z., Zhu, Y., 2005. Adsorption thermodynamic, kinetic and desorption studies of Pb^{2+} on carbon nanotubes. Wat. Res. 39, 605–609.
López-García, M., Martínez-Cabanas, M., Vilariño, T., Lodeiro, P., Rodríguez-Barro, P., et al., 2017. New polymeric/inorganic hybrid sorbents based on red mud and nanosized magnetite for large scale applications in As (V) removal. Chem. Eng. J. 311, 117–125.
Lǔ, J., Liu, H., Liu, R., Zhao, X., Sun, L., et al., 2013. Adsorptive removal of phosphate by a nanostructured Fe-Al-Mn trimetal oxide adsorbent. Powder Technol. 233, 146–154.
Mahmoodi, N.M., Khorramfar, S., Najafi, F., 2011. Amine-functionalized silica nanoparticle: preparation, characterization and anionic dye removal ability. Desalination 279, 61–68.
Mezenner, N.Y., Bensmaili, A., 2009. Kinetics and thermodynamic study of phosphate adsorption on iron hydroxide-eggshell waste. Chem. Eng. J. 147 (2–3), 87–96.
Mor, S., Chhoden, K., Ravindra, K., 2016. Application of agro-waste rice husk ash for the removal of phosphate from the wastewater. J. Clean. Prod. 129, 673–680.
Nethaji, S., Sivasamy, A., Mandal, A.B., 2013. Adsorption isotherms, kinetics and mechanism for the adsorption of cationic and anionic dyes onto carbonaceous particles prepared from Juglans regia shell biomass. Int. J. Environ. Sci. Technol. 10 (2), 231–242.
Radnia, H., Ghoreyshi, A.A., Younesi, H., 2011. Isotherm and kinetics of Fe (II) adsorption onto chitosan in a batch process. Iranica Journal of Energy & Environment 2 (3), 250–257.
Razzaque, M.S., 2011. Phosphate toxicity: new insights into an old problem. Clin. Sci. (Lond). 120, 91–97.
Sahu, M.K., Mandal, S., Dash, S.S., Badhai, P., Patel, R.K., 2013. Removal of Pb(II) from aqueous solution by acid activated red mud. J. Environ. Chem. Eng. 1, 1315–1324.
Sips, R., 1948. On the structure of a catalyst surface. J. Chem. Phys. 16, 490–495.
Vithanage, M., Mayakaduwa, S.S., Herath, I., Ok, Y.S., Mohan, D., 2016. Kinetics, thermodynamics and mechanistic studies of carbofuran removal using biochars from tea waste and rice husks. Chemosphere 150, 781–789.
Wang, L., Liang, T., 2015. Distribution characteristics of phosphorus in the sediments and overlying water of Poyang Lake. PLoS One 10, e0125859.
Wang, S., Boyjoo, Y., Choueib, A., Zhu, Z.H., 2005. Removal of dyes from aqueous solution using fly ash and red mud. Water Res. 39 (1), 129–138.
Wang, S., Wang, K., Dai, C., Shi, H., Li, J., 2015. Adsorption of Pb^{2+} on amino-functionalized core–shell magnetic mesoporous SBA-15 silica composite. Chem. Eng. J. 262, 897–903.
Wang, Y., Yu, Y., Li, H., Shen, C., 2016. Comparison study of phosphorus adsorption on different waste solids: Fly ash, red mud and ferric–alum water treatment residues. J. Environ. Sci. 50, 79–86.
Weis, J.S., Weis, P., 2004. Metal uptake, transport and release by wetland plants: implications for phytoremediation and restoration. Environ. Int. 30, 685–700.
Wimalasiri, Y., Mossad, M., Zou, L., 2015. Thermodynamics and kinetics of adsorption of ammonium ions by graphene laminate electrodes in capacitive deionization. Desalination 357, 178–188.
Yao, Y., Gao, B., Inyang, M., Zimmerman, A.R., Cao, X., et al., 2011. Removal of phosphate from aqueous solution by biochar derived from anaerobically digested sugar beet tailings. J. Hazard. Mater. 190, 501–507.
Yildiz, E., 2004. Phosphate removal from water by fly ash using crossflow microfiltration. Sep. Purif. Technol. 35, 241–252.
Zhao, T.L., Li, H., Huang, Y.R., Yao, Q.Z., Huang, Y., Zhou, G.T., 2019. Microbial mineralization of struvite: salinity effect and its implication for phosphorus removal and recovery. Chem. Eng. J. 358, 1324–1331.
Zheng, Y., Zhu, B., Chen, H., You, W., Jiang, C., Yu, J., 2017. Hierarchical flower-like nickel (II) oxide microspheres with high adsorption capacity of Congo red in water. J. Colloid Interface Sci. 504, 688–696.